Turner, Stuart M.R. and Bridges, John C. and Grebby, Stephen and Ehlmann, Bethany L. (2016) Hydrothermal activity recorded in post Noachian-aged impact craters on Mars. Journal of Geophysical Research: Planets, 121 (4). pp. 608-625. ISSN 2196-9100

AGU PUBLICATIONS

JGR

Journal of Geophysical Research: Planets

RESEARCH ARTICLE
10.1002/2015JE004989

Key Points:
- Mars craters in post Noachian terrains studied with CRISM to determine presence of hydrated minerals
- Only 3 of 158 craters show clay-bearing assemblages
- Impact hydrothermalism possible in two craters

Supporting Information:
- Supporting Information S1
- Table S1

Correspondence to:
J. C. Bridges,
j.bridges@leicester.ac.uk

Citation:
Turner, S. M. R., J. C. Bridges, S. Grebby, and B. L. Ehlmann (2016), Hydrothermal activity recorded in post Noachian-aged impact craters on Mars, *J. Geophys. Res. Planets*, *121*, 608–625, doi:10.1002/2015JE004989.

Received 11 DEC 2015
Accepted 10 MAR 2016
Accepted article online 16 MAR 2016
Published online 15 APR 2016

Hydrothermal activity recorded in post Noachian-aged impact craters on Mars

Stuart M. R. Turner[1], John C. Bridges[1], Stephen Grebby[2], and Bethany L. Ehlmann[3]

[1]Space Research Centre, Department of Physics and Astronomy, University of Leicester, Leicester, UK, [2]British Geological Survey, Nottingham, UK, [3]Division of Geological and Planetary Sciences and Jet Propulsion Laboratory, California Institute of Technology, Pasadena, California, USA

Abstract Hydrothermal systems have previously been reported in ancient Noachian and Hesperian-aged craters on Mars using CRISM but not in Amazonian-aged impact craters. However, the nakhlite meteorites do provide evidence of Amazonian hydrothermal activity. This study uses CRISM data of 144 impact craters of ≥7 km diameter and 14 smaller craters (3–7 km diameter) within terrain mapped as Amazonian to search for minerals that may have formed as a result of impact-induced hydrothermal alteration or show excavation of ancient altered crust. No evidence indicating the presence of hydrated minerals was found in the 3–7 km impact craters. Hydrated minerals were identified in three complex impact craters, located at 52.42°N, 39.86°E in the Ismenius Lacus quadrangle, at 8.93°N, 141.28°E in Elysium, and within the previously studied Stokes crater. These three craters have diameters 20 km, 62 km, and 51 km. The locations of the hydrated mineral outcrops and their associated morphology indicate that two of these three impact craters—the unnamed Ismenius Lacus Crater and Stokes Crater—possibly hosted impact-induced hydrothermal systems, as they contain alteration assemblages on their central uplifts that are not apparent in their ejecta. Chlorite and Fe serpentine are identified within alluvial fans in the central uplift and rim of the Ismenius Lacus crater, whereas Stokes crater contains a host of Fe/Mg/Al phyllosilicates. However, excavation origin cannot be precluded. Our work suggests that impact-induced hydrothermalism was rare in the Amazonian and/or that impact-induced hydrothermal alteration was not sufficiently pervasive or spatially widespread for detection by CRISM.

1. Introduction

Understanding the history, nature, and occurrence of hydrated minerals in the Martian crust is key to identifying potential past habitable environments. Recent investigations carried out using the Mars Exploration Rovers (MER), Mars Express (MEX), Mars Reconnaissance Orbiter (MRO), and Mars Science Laboratory (MSL) have revealed hydrated minerals in a diverse range of environments [e.g., *Squyres et al*., 2004; *Bibring et al*., 2006; *Poulet et al*., 2007; *Ehlmann et al*., 2009; *Murchie et al*., 2009a; *Grotzinger et al*., 2014; *Ehlmann and Edwards*, 2014]. Furthermore, remote sensing studies using the OMEGA (Observatoire pour la Minéralogie, l'Eau, les Glaces et l'Activité) and CRISM (Compact Reconnaissance Imaging Spectrometer for Mars) visible to infrared spectrometers on MEX and MRO, respectively, have identified phyllosilicates predominantly in ancient Noachian era terrains of Mars [*Poulet et al*., 2005; *Mustard et al*., 2008; *Ehlmann et al*., 2011a; *Carter et al*., 2013]. These studies, along with others [e.g., *Marzo et al*., 2010; *Mangold et al*., 2012; *Osinski et al*., 2013], have reported evidence of hydrothermal minerals associated with numerous craters formed in the Noachian and Hesperian terrains, mostly via excavation of older altered material, but with impact-induced hydrothermalism occurring in a small number of craters.

Here we investigate nominally Amazonian terrains to determine how widespread impact-associated secondary mineral assemblages within post Noachian craters are and to compare the mineralogy and geologic setting of these assemblages with those in more ancient cratered terrains. The goal is to assess the timing and frequency of occurrence of hydrothermal activity in the Amazonian.

1.1. Remote Sensing of Mars With OMEGA and CRISM

In early studies, the OMEGA visible-shortwave infrared imaging spectrometer was utilized to map hydrated mineral exposures at a spatial resolution (pixel size) of 1.8 km, resulting in the identification of three types of hydrated minerals—Fe/Mg phyllosilicates, Al phyllosilicates, and hydrated sulfates—at five locations on Mars: Terra Meridiani, Mawrth Vallis, Nili Fossae, Aram Chaos, and Valles Marineris along with scattered other highland locations [*Bibring et al*., 2006; *Poulet et al*., 2007]. Interpreting OMEGA observations in the context of

the geological history of Mars, *Poulet et al*. [2005] suggested that formation of phyllosilicates occurred predominantly during the early Noachian, followed by a more acidic environment in which sulfate formation was prevalent. In a subsequent study, *Bibring et al*. [2006] proposed three distinct eras of alteration based on OMEGA observations—"Phyllosian," "Theiikian," and "Siderikian"—characterized by phyllosilicates, sulfates, and ferric oxides, respectively. These three eras can be loosely linked to the Noachian, Hesperian, and Amazonian epochs [*Bibring et al*., 2006]. *Mustard et al*. [2005] reported that OMEGA data in the northern plains of Mars lack strong mafic absorptions as well as absorptions due to hydrated minerals but suggested that surface coatings could mask such signatures.

More recently, higher-resolution hyperspectral imagery of Mars has been acquired by the CRISM instrument at 18–40 m/pixel [*Murchie et al*., 2007, 2009a, 2009b]. The higher spatial resolution of CRISM in comparison to OMEGA has resulted in the identification of numerous hydrated mineral exposures coupled with deposit morphology, thus enabling a more detailed understanding of Mars's surface mineralogy and providing insights about past environmental conditions. Phyllosilicates, predominantly Fe/Mg smectites, have been detected in layered sediments (Al smectite is also present), intracrater fans, plains sediments, and basement/exhumed deposits (also known as "deep phyllosilicates") [*Mustard et al*., 2008; *Murchie et al*., 2009a]. Many of these deposits contain minerals formed in hydrothermal environments such as chlorite ($(Mg,Fe)_5Al(AlSi_3)O_{10}(OH)_8$), prehnite ($Ca_2Al_2Si_3O_{10}(OH)_2$), serpentine ($(Mg, Fe)_3Si_2O_5(OH)_4$), and zeolites [*Mustard et al*., 2008; *Ehlmann et al*., 2009, 2011b]. Hydrated sulfate mineral deposits have been detected in intracrater clay-sulfate deposits, Meridiani-type layered deposits, valles-type layered deposits, siliceous layered deposits, and gypsum plains [*Murchie et al*., 2009a]. Carbonate deposits have also been detected, more rarely, with CRISM data in Noachian terrains [*Ehlmann et al*., 2008, 2009; *Murchie et al*., 2009a; *Carter and Poulet*, 2012; *Bultel et al*., 2015]. Analysis of CRISM data has also helped guide landing site selection and rover-based investigations on MER and MSL. Moreover, CRISM analyses of Gale crater indicated clay deposits [*Milliken et al*., 2010; *Thomson et al*., 2011] consistent with X-ray diffraction measurements taken on board MSL to date [*Bish et al*., 2014; *Vaniman et al*., 2014]. These deposits formed largely through burial diagenesis of basaltic sediments rather than impact-induced alteration [*McLennan et al*., 2014; *Bridges et al*., 2015].

In situ investigations carried out by the MER program have also uncovered evidence of aqueous alteration. Specifically, the MER Opportunity rover has identified the presence of acid groundwater-fed sabkha-type deposits rich in sulfates, along with veins of various phyllosilicate minerals and Ca-sulfate within Noachian materials exposed in Endeavour crater [*Arvidson et al*., 2014]. The MER Spirit rover has revealed evidence for hydrothermal activity in the Gusev crater floor [*Ming et al*., 2006; *Squyres et al*., 2008; *Morris et al*., 2010; *Filiberto and Schwenzer*, 2013], although there is no clear link to heat released from the Gusev impact. The in situ measurements made by MER Spirit at Gusev crater are consistent with CRISM observations [*Carter and Poulet*, 2012].

1.2. Theory of Impact-Induced Hydrothermal Activity

A hypervelocity impact into a planetary crust produces a shock wave that compresses and transfers a large amount of energy to the crust. This shock event is not thermodynamically reversible: upon decompression of the planetary crust by rarefaction waves, waste heat is produced which raises the temperature of the planetary crust [*Melosh*, 1989]. On Mars, a central uplift is more likely to form for impact craters above 7 km diameter, caused by the rise of deep-seated rocks located beneath the crater as it returns to a state of gravitational equilibrium during the later stages of impact crater formation. The existence of this central structure classifies the crater as complex [*Melosh*, 1989; *Abramov and Kring*, 2005]. The uplift of warm, deep-seated material can, if the crust is water- or ice-rich, establish subsurface convection cells of water that alter the surrounding rock to produce phyllosilicate-rich alteration phases [*Schwenzer and Kring*, 2009]. The longevity of such impact-induced hydrothermal systems depends on the physical and kinetic properties of the impactor, permeability of the planetary crust, and the subsequent size and type of the resultant impact crater [*Abramov and Kring*, 2005; *Barnhart et al*., 2010; *Rathbun and Squyres*, 2002]. In simple craters ($<$ ~7 km on Mars), shock-emplaced heat dominates due to the lack of a central uplift and a negligible amount of impact melt; thus, convection cells cannot be easily established.

Research has suggested that subsurface impact-induced hydrothermal activity in the volatile-bearing crust of Mars has the potential to last for 67,000 years for a 30 km diameter crater, 290,000 years for a 100 km diameter

crater, and up to ~10 Myr for craters the size of the Hellas basin (~2000 km diameter) [*Abramov and Kring*, 2005]. The prolonged period of time that the host rock is subjected to heat and water suggests that an impact-induced hydrothermal system can produce and sustain a habitable environment for microbial life [*Rathbun and Squyres*, 2002; *Abramov and Kring*, 2005; *Cockell et al*., 2012].

1.3. Evidence for Impact-Induced Hydrothermal Activity on Mars

Spectral evidence for impact-induced hydrothermal systems on Mars is scarce, with the oldest of the possible examples being the ~153 km diameter Noachian-aged Holden impact crater (−26.04°N, 325.98°E) located in the Margaritia Sinus quadrangle, within which extensive erosion of the ejecta and southwest rim/terraces of the crater has exposed megabreccias, interpreted as pre-Holden materials excavated by impact [*Grant et al*., 2008]. *Tornabene et al*. [2009] and *Osinski et al*. [2013] utilized HiRISE and CRISM data to show that light-toned fractures within the megabreccia exhibit absorptions at ~1.9 μm and ~2.3 μm, indicating the presence of Fe/Mg clays. *Osinski et al*. [2013] suggested that these secondary mineral-bearing fractures are indicative of impact-induced hydrothermal alteration.

More recent impact-induced hydrothermal activity has been suggested for the ~40 km diameter Hesperian-aged Toro complex impact crater (17.04°N, 71.83°E) in the Syrtis Major quadrangle, with prehnite, chlorite, smectites, and opaline materials detected in impact-melt-bearing crater fill deposits along, in, and around the central uplift as well as in the ejecta [*Ehlmann et al*., 2009; *Marzo et al*., 2010; *Osinski et al*., 2013]. *Marzo et al*. [2010] proposed a model of impact excavation and impact-induced hydrothermal activity for Toro crater, given morphologic features within the central peak consistent with hydrothermal systems and hydrated minerals within the crater central peak and floor. However, *Ehlmann et al*. [2009, 2011b] mapped the same minerals both inside and outside the crater peak and argued for their origin by excavation of hydrothermally altered materials that predated the crater.

Majuro crater (−33.26°N, 84.35°E), on the northeastern Hellas basin rim, represents another example of potential impact-induced hydrothermal alteration during the Hesperian and perhaps provides the strongest evidence for such a system to date. Available MRO and MEX coverage of this ~45 km diameter late-Hesperian-aged complex impact crater reveals Fe/Mg phyllosilicates and opaline silica in the crater rims, floor, and central peak [*Mangold et al*., 2012]. This crater also contains a 20 km long alluvial fan extending from the crater wall to the floor at the base of the central uplift that has an unaltered northern upper section and an altered lower section. *Mangold et al*. [2012] concluded that the altered minerals in the fan most likely formed following hydrothermal circulation initiated by the crater-forming impact and subsequent redeposition by physical weathering in the alluvial fan.

An impact-induced hydrothermal alteration hypothesis has also been proposed for the ~50 km diameter Micoud complex impact crater (50.58°N, 16.35°E) located in the late-Hesperian-aged [*Tanaka et al*., 2014] Vastitas Borialis formation in the northern plains, where the presence of prehnite in and around the central uplift is shown with CRISM data [*Gross et al*., 2012]. Hydrated silica deposits and Fe/Mg phyllosilicates in the central uplift of 78 km diameter Ritchey crater (−28.5°N, 309°E), which formed in the Hesperian, have been shown to postdate the impact and may result from impact-induced aqueous alteration [*Sun and Milliken*, 2014].

Collectively, the CRISM data indicate that subsurface hydrothermal processes were widespread; found in excavated Noachian crust from hundreds of craters [*Mustard et al*., 2008; *Ehlmann et al*., 2011a, 2011b]. Definitively, impact-induced hydrothermal processes—arguably harder to uniquely identify from orbit—are restricted to a few candidate locations, the most outstanding of which is a late Hesperian crater.

1.3.1. The Nakhlite Martian Meteorites

Evidence for hydrated, secondary minerals is also found in the Martian Shergottite, Nakhlite, and Chassigny (SNC) meteorites, most notably in the nakhlite group [*Gooding et al*., 1991; *Bridges and Grady*, 2000; *Changela and Bridges*, 2010; *Bridges and Schwenzer*, 2012; *Hicks et al*., 2014]. Formed on Mars in the Amazonian, ~1.3 Ga, in a basic-ultrabasic lava flow or shallow intrusion (~100 m), these basaltic cumulate clinopyroxenite rocks have veins within brittle impact-induced fractures that contain the alteration minerals: ferric saponite ($(Ca_{0.25}(Mg,Fe)_3((Si,Al)_4O_{10})(OH)_2 \cdot n(H_2O))$, ferric serpentine, siderite ($FeCO_3$), a gel/poorly crystalline saponite, and salts [*Gooding et al*., 1991; *Bridges and Grady*, 2000; *Changela and Bridges*, 2010; *Hicks et al*., 2014]. Truncation of these veins by the fusion crust indicates a preterrestrial (Martian) origin [*Gooding et al*., 1991].

Poorly crystalline materials located within fractured olivine ($(Mg, Fe)_2SiO_4$) and mesostasis indicates that the nakhlites underwent rapid cooling. Together with the veining within the brittle fractures—which suggests the presence of shock effects (though of lesser magnitude than seen in the shergottites [*Nyquist et al*., 2001])—this suggests that the nakhlite parent body may have been at the margins of a short-lived Amazonian era impact-induced hydrothermal system [*Changela and Bridges*, 2010]. Computer modeling with the program CHILLER showed that the nakhlite alteration assemblage formed from a potentially habitable neutral to alkaline brine with a peak temperature ≤150–200°C in a near-surface setting, with Ca-rich siderite precipitating at these high temperatures and saponite and serpentine precipitating once the fluid had cooled to ~50°C [*Bridges and Schwenzer*, 2012]. K-Ar dating of alteration products (i.e., smectite- and siderite-veined olivine grains) suggests that this fluid activity occurred ≤670 Myr [*Shih et al*., 1998; *Swindle et al*., 2000].

1.4. This Study

In this paper we use CRISM data acquired for impact craters emplaced within Amazonian terrains to assess the extent to which evidence of hydrothermal alteration of post Noachian-aged materials is present. Using the latest USGS Geologic Map of Mars [*Tanaka et al*., 2014] as a guide, we have analyzed 282 CRISM images covering 158 craters in the northern hemisphere of Mars. As a result, three craters have been found to exhibit compelling spectral features that indicate the presence of hydrated minerals, two of which may have evidence for postimpact hydrothermal systems.

2. Methods

2.1. The CRISM, HiRISE, CTX, and MOLA Instruments

The CRISM instrument on board MRO is a visible/shortwave infrared imaging spectrometer, which in targeted mode acquires 18–40 m/pixel images of ~10 × 3–20 km areas from 362 nm to 3920 nm over 544 channels, with a spectral sampling of 6.55 nm/channel. This is achieved using a gimbaled optical sensor unit to compensate for the orbital motion of MRO, allowing for a long acquisition time (2–3 min) of a targeted area and acquisition of data with a high signal-to-noise ratio [*Murchie et al*., 2007]. CRISM also images the Martian surface in a mapping mode, where the instrument acquires 100–200 m/pixel nadir images of ~10 km in width and ≤550 km long [*Murchie et al*., 2007].

High-resolution imagery provides geological context for the mineral detections. Accordingly, imagery acquired by the High Resolution Imaging Science Experiment (HiRISE) and Context Camera (CTX)—both also on board MRO—were utilized for this purpose. The HiRISE instrument is capable of acquiring 0.3 m/pixel images at 300 km altitude [*McEwen et al*., 2007], whereas CTX can acquire 6 m/pixel images at 300 km altitude [*Malin et al*., 2007].

Topographic data from the Mars Orbiter Laser Altimeter (MOLA), on board the Mars Global Surveyor, was obtained and used to provide profiles of impact craters and to help ascertain the depth of the mineral signatures of interest. MOLA successfully mapped the topography of Mars with a vertical accuracy of 1 m and along-track shot spacing of 300 m with spot size of 168 m at 400 km elevation mapping orbit [*Smith et al*., 2001]. The resultant topographic map of Mars has a resolution of 128 pixels per degree, and we use profiles extracted from this global map.

2.2. Identification of Candidate Craters

The impact craters were identified using a combination of the geologic map of Mars [*Tanaka et al*., 2014], the *Robbins and Hynek* [2012] crater database, MOLA topographic data, and CTX imagery. The analysis approach taken involved cropping the *Robbins and Hynek* [2012] crater database to units mapped as Amazonian in the USGS Mars quadrangles, and then systematically searching each quadrangle for applicable impact craters with high-resolution CRISM scenes: FRS, FRT, HRL, and HRS (Full Resolution Short, Full Resolution Targeted, Half Resolution Long, and Half Resolution Short, respectively). Applicable candidate craters were defined as those that had distinct and complete crater walls and floors/central uplifts. Filled-in craters were excluded from this study because of the difficulty in identifying potential impact-induced hydrothermal alteration beneath the infill material using CRISM data.

Initially, impact craters with diameters ≥7 km were selected for analysis as this represents the transition diameter from simple to complex impact craters, where impact-induced hydrothermal systems are more likely

to occur [*Daubar and Kring*, 2001; *Abramov and Kring*, 2005]. Impact crater diameters were extracted from the *Robbins and Hynek* [2012] crater database.

A secondary survey of smaller impact craters was carried out on impact craters ≥3 km and <7 km. This extends the selection to include simple craters, for which the shock-emplaced heat would be the dominant heat source [*Schwenzer and Kring*, 2013] and impacts large enough to eject material from the surface of Mars [*Head et al*., 2002]. Large outcrops of postimpact-generated hydrated minerals would be unlikely for simple craters as shock-emplaced heat would dominate, resulting in smaller hydrous mineral deposits within outcrops, as opposed to widespread alteration driven by a hydrothermal cell. Smaller outcrops with hydrous minerals are more likely to be restricted to rocky interiors or masked by later fill or dust, and so additional selection criteria based on Thermal Emission Spectrometer (TES) dust coverage was introduced. Only craters with TES dust coverage index (1350–1400 cm^{-1} average emissivity) >0.94 [*Ruff and Christensen*, 2002], indicating minimum dust coverage, were studied.

2.3. CRISM Data Processing and Spectral Identification of Minerals

Raw CRISM data were converted to I/F [*Murchie et al*., 2009b] and obtained from the NASA Planetary Data System Geosciences Node. The data were subsequently processed and analyzed using the CRISM Analysis Toolkit (CAT) version 7.2.1, a software tool released by the CRISM team that is an extension to the Environment for Visualizing Images (ENVI) software package. Photometric effects were corrected by division of the cosine of the incidence angle of the observation, and atmospheric effects were corrected using the volcano scan method [*McGuire et al*., 2009]. Summary products [*Pelkey et al*., 2007] were then calculated and used to identify regions with spectral properties of interest, along with a corresponding spectrally bland region. The region of interest was ratioed to a bland patch within the same image columns to divide out the systematic instrument artifacts and residuals from the atmospheric correction in the spectrum of interest, accentuating compositional differences between the regions. This conventional method of spectral extraction from CRISM data has been used in several previous studies [e.g., *Ehlmann et al*., 2009; *Milliken et al*., 2010].

Mafic, nonhydrated minerals were highlighted by deriving olivine and high- and low-calcium pyroxene (OLINDEX, LCPINDEX, and HCPINDEX) summary parameters from the CRISM imagery. Olivine, $(Fe,Mg)_2SiO_4$, was identified by characteristic absorptions in its spectrum at ~1.0 μm, which are caused by crystal field transitions of Fe^{2+} [*Burns*, 1970]. In contrast, the spectrum of the pure forsterite end-member (Mg_2SiO_4) is featureless [*Adams*, 1975]. Pyroxenes, $(Ca,Fe,Mg)_2Si_2O_6$, generally have two characteristic bands that shift depending on Ca and Fe content—low-Ca pyroxenes tend to have a strong absorption at 0.9 μm and a broad absorption 1.8 μm, which are shifted to 1.0 μm and 2.3 μm for high-Ca pyroxenes with an increasing Fe content [*Adams*, 1975; *Mustard et al*., 2005].

Hydrated minerals were initially identified by a diagnostic spectral feature at 1.9 μm, which is attributed to combinations of bending and stretching vibrations of H_2O within the mineral structure. Combination overtones of H_2O, along with OH overtones caused by structural stretching vibrations, result in an absorption at ~1.4 μm. In phyllosilicates, the position of the OH overtone is influenced by the octahedral cation present causing it to shift between 1.38 and 1.43 μm [*Bishop et al*., 2008]. Absorptions between 2.0 and 2.6 μm are most indicative of the hydrated silicate phase present. More specifically, Al-OH and Si-OH absorptions occur at ~2.21 μm, whereas Fe-OH and Mg-OH absorptions occur at ~2.29 μm and ~2.32 μm, respectively [*Bishop et al*., 2002a, 2002b]. Monohydrated sulfates have a broad absorption band at ~2.0 μm with a diagnostic absorption band at 2.4 μm, whereas polyhydrated sulfates have absorption bands around 1.4 μm and 1.9 μm, consistent with H_2O and OH overtones, with a dropoff near 2.4 μm [*Cloutis et al*., 2006]. Carbonates have absorption bands around 2.3 μm and 2.5 μm, but their exact position depends on the major cation. Mg-rich carbonates have absorption bands at 2.30 μm and 2.50 μm, Ca-rich carbonates have absorption bands at 2.34 μm and 2.54 μm, and Fe-rich carbonates have absorption bands at 2.33 μm and 2.53 μm [*Gaffey*, 1987]. H_2O ice has diagnostic absorption bands at 1.25 μm, 1.5 μm, and 2.0 μm, whereas CO_2 ice has 1.435 μm and 2.281 μm absorptions [*Langevin et al*., 2007].

2.4. Definition of a "Null" Result

A "Null" result in this study is defined as an impact crater that meets the criteria previously outlined but CRISM analysis did not reveal the presence of hydrated minerals. For clarification, this does not definitively rule out

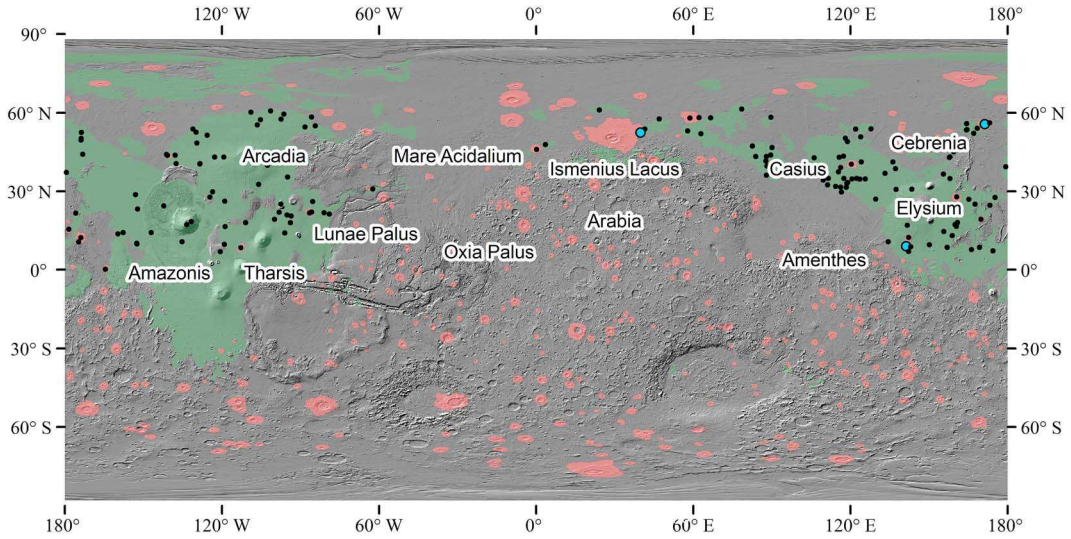

Figure 1. Grayscale MOLA map showing the impact craters analyzed in this study. Amazonian-Hesperian terrains are highlighted in green, with Amazonian-Hesperian Impact (AHi) units highlighted in red. Only AHi units overlying Amazonian-Hesperian terrains were considered in this study; map units from *Tanaka et al.* [2014]. CRISM data from 158 impact craters were studied, with three craters showing evidence of hydrated minerals. Black dots indicate impact craters that did not show hydrated minerals; blue dots indicate impact craters that contain hydrated minerals.

the presence of hydrated minerals, but rather simply indicates the inability to identify them using the CRISM data at 18–40 m/pixel scale and with the possibility of dust cover.

3. Results

Following analyses of 267 CRISM images covering 144 craters ≥7 km diameter in the northern hemisphere of Mars, just three craters were found to show compelling spectral features suggesting the presence of hydrated silicate minerals (Figure 1). No sulfate minerals were found in this study. The locations and associated diameters of these three impact craters are detailed in Table 1. An additional 15 CRISM images covering 14 impact craters of diameters ≥3 km and <7 km in relatively dust-free Amazonian mapped terrain units in the Northern Plains were also analyzed, but no evidence for the presence of hydrated minerals was found. There was no CRISM coverage for candidate impact craters found in Amazonian terrains in west Hellas Basin. Table S1 in the supporting information shows the full list of impact craters and associated CRISM images analyzed in this study.

3.1. Unnamed Ismenius Lacus Impact Crater

This unnamed, ~20 km diameter impact crater, known as 05-000375 in the *Robbins and Hynek* [2012] crater database, is a complex impact crater located at 52.42°N, 39.86°E in the Ismenius lacus quadrangle of Mars (Figure 2). The terrain impacted is mapped as an Amazonian-Hesperian-aged unit [*Tanaka et al.*, 2014] and a recent study used crater counts to date this crater as 0.3 Ga [*Sun and Milliken*, 2015]. The impact crater has a pronounced central uplift with a maximum diameter of 4.9 km and radial, multilayered, fluidized ejecta previously noted as hummocky with broad lobes [*Robbins and Hynek*, 2012]. The crater floor has a minimum MOLA elevation of −4.49 km with an overall crater depth of 1.2 km with respect to the crater rim. Inspection

Table 1. Amazonian Impact Craters With Phyllosilicates Found in This Study

Name	Quadrangle	Crater ID[a]	Diameter (km)	Latitude (°N)	Longitude (°E)
Unnamed	Ismenius Lacus	05-000375	20.0	52.42	39.86
Unnamed	Elysium	15-000018	50.8	8.93	141.28
Stokes	Cebrenia	07-000008	62.5	55.62	171.23

[a]Crater ID refers to the crater identification tag in *Robbins and Hynek* [2012].

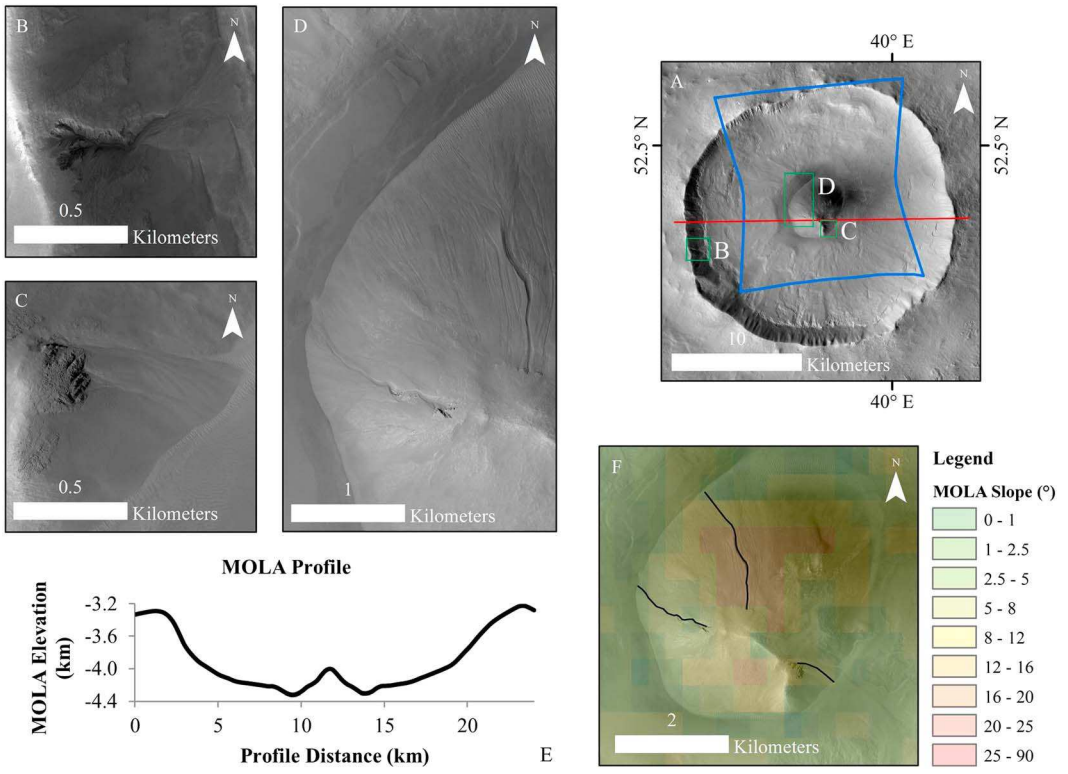

Figure 2. The 20 km complex impact crater located 52.42°N, 39.86°E in the Ismenius Lacus quadrangle of Mars. (a) CTX B02_010260_2327 with CRISM FRT0000BFA6 outline (blue) and location of the MOLA profile (red) overlain. (b) Alluvial fan located on western crater wall in HiRISE ESP_040958_2325. (c) Alluvial fan located on the southwest region of the central uplift in HiRISE PSP_009561_2325. (d) Alluvial fans located on the northern and western regions of the central uplift in HiRISE PSP_009561_2325 showing dark-toned material indicating possible recent movement of material within the gully. (e) MOLA profile of the crater illustrated in Figure 2a by the red line. (f) MOLA-derived slope map of central uplift showing that the largest gully (gullies/fans tracked with black lines) on the northern region of the central uplift has formed where the slope is greatest.

of HiRISE PSP_009561_2325 and ESP_040958_2325 showed evidence for four alluvial fans in the wall and central peak (Figures 2b–2d).

Four CRISM scenes cover the impact crater: FRT0000BFA6, FRT0001B619, HRL000194F4, and HRL0001B89D. Summary products derived from FRT0000BFA6 indicated absorptions at ~1.9 μm and ~2.3 μm in materials in the central structure, both in rocky materials and in alluvial fans on the central uplift of the impact crater (Figures 2c, 2d, and 3). Further analysis of continuum-removed CRISM spectra (Figure 3) revealed a 1.92–1.94 μm absorption, indicating the presence of molecular H_2O, in addition to an absorption centered at 2.35 μm and a shoulder at ~2.2–2.3 μm for spectra of fan #1 and megabreccia material. The spectra for the fan #1 material also has an absorption at ~1.48 μm that together with the other absorptions present in this spectra suggest the possibility of prehnite. For all spectra present in Figure 3, the absorptions indicate the presence of Fe/Mg phyllosilicates, possibly Fe serpentines, or chlorites. A broad absorption centered near 1.25 μm indicates the presence of iron, either in an Fe-bearing igneous mineral or in the Fe/Mg phyllosilicate phase. The hydrous signatures are confined to the central structure, including probable megabreccia blocks, rocky alcoves at the head of each of the gullies, and alluvial fans (Figure 3) but do not extend on to the crater floor. Sands within the crater are enriched in mafic minerals.

A MOLA profile of the crater was extracted (Figure 2e) and a slope map derived from the 128 pixels per degree MOLA topographic map of Mars, using the slope tool within the ArcGIS spatial analyst toolbox (Figure 2f). The northern gully/alluvial fan has a slope maximum of 14.7° and a minimum of 4.5°, whereas the western gully/alluvial fan has a slope maximum of 6.4° and a minimum of 3.3°. The smaller fan shown in Figure 2c has a slope maximum of 7.8° and a minimum of 4.0°. In this study gullies are observed on pole-, eastern, and western facing slopes. In contrast, a study of the Northern Hemisphere showed that gullies at

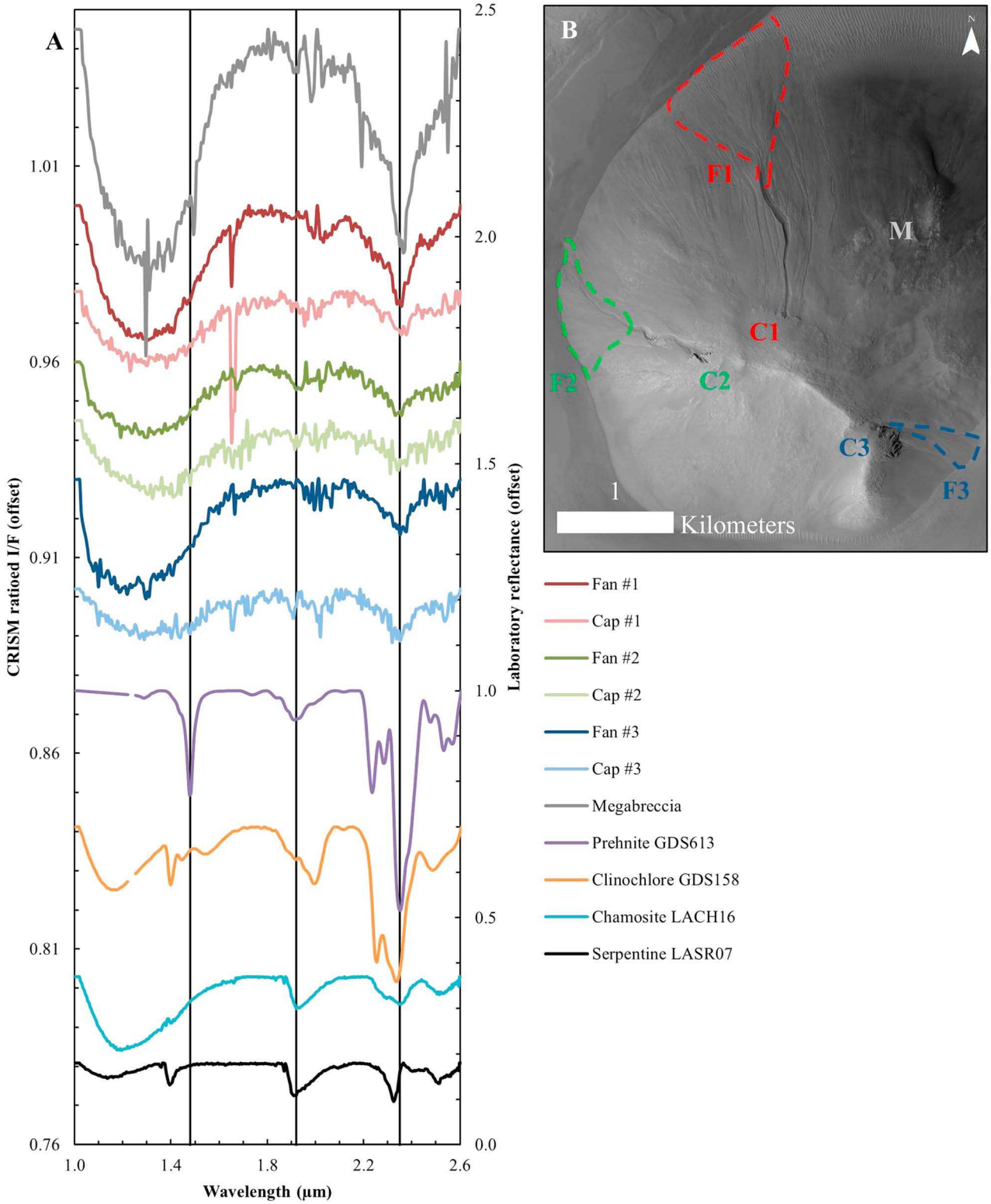

Figure 3. The 20 km complex impact crater located 52.42°N, 39.86°E in the Ismenius Lacus quadrangle of Mars. (a) CRISM continuum-removed spectra extracted from FRT0000BFA6 of fans shown in Figure 3b. The 1.92–1.94 μm and 2.351 μm absorptions indicate the presence of chlorite/Fe-serpentine /prehnite. Apparent absorptions at 1.65 and 2.0 μm are caused by a filter boundary and residual atmospheric absorptions, respectively. Laboratory spectra are from the USGS spectral library [*Clark et al.*, 2007]. (b) HiRISE PSP_009561_2325_RED showing gullies and fans in the central uplift, with areas of CRISM spectral extraction outlined. Fans 1–3 are sized 0.73 km^2 (1817 CRISM pixels), 0.28 km^2 (705 CRISM pixels), and 0.14 km^2 (358 CRISM pixels), respectively. Caps #1–3 and megabreccia spectra shown in Figure 3a are sized 400, 55, 80, and 91 CRISM pixels, respectively.

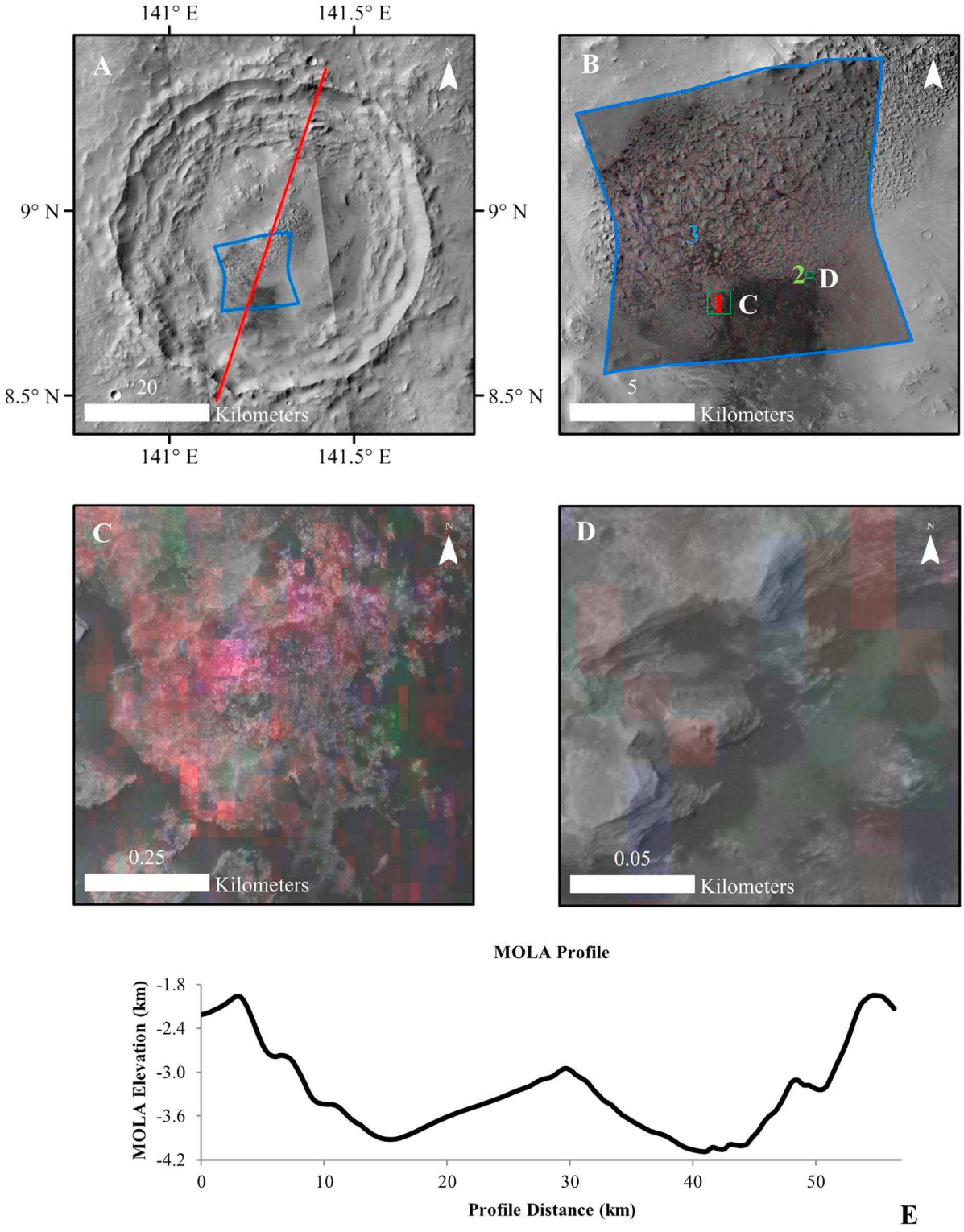

Figure 4. The ~51 km diameter unnamed complex impact crater located 8.93°N, 141.28°E in the Elysium quadrangle of Mars. (a) CTX mosaic showing the impact crater with CRISM FRT0000619D outline (blue) and location of the MOLA profile (red) overlain. (b) CTX mosaic with CRISM FRT0000619D RGB parameter map [*Pelkey et al.*, 2007] composite D2300 (red), BD2210 (green), and BD1900 (blue). Context locations for zoomed views in Figures 4c and 4d are indicated by the green boxes. Context locations for spectra in Figure 5 are shown by 1, 2 (from within green boxes), and 3. (c) HiRISE ESP_043051_1890_RED overlain with CRISM RGB parameter map (shown in Figure 4b) reveals areas of mixed absorptions (1.9 μm and 2.3 μm highlighted by purple). (d) Close-up of central uplift in a portion of HiRISE PSP_008305_1890_RED (overlain with CRISM RGB parameter map shown in Figure 4b), showing the morphology of the central uplift, proposed to be eroded crater fill. (e) MOLA profile of the crater illustrated in Figure 4a by the red line.

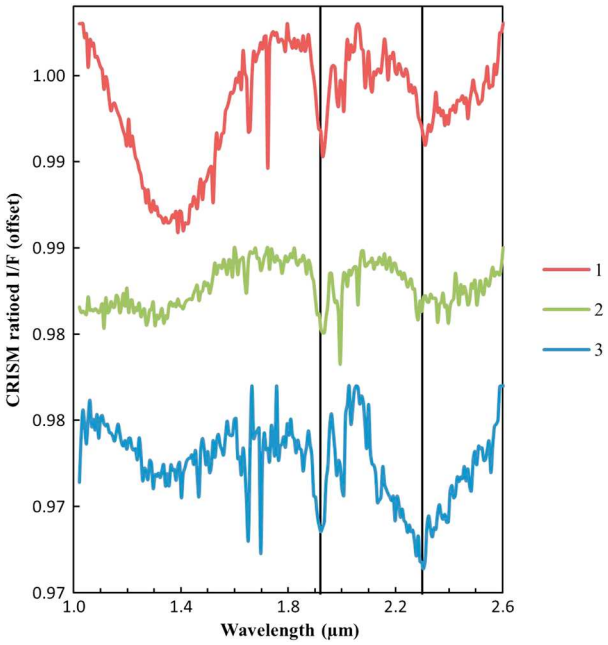

Figure 5. CRISM continuum-removed spectra extracted from FRT0000619D of eroded crater fill in Elysium impact crater, shown in Figures 4b and 4c. The spectra show 1.92–1.93 μm and 2.29–2.31 μm absorptions, which are consistent with Fe/Mg phyllosilicates.

this latitude tend to form on equator-facing slopes [*Heldmann et al.*, 2007]. Slope length from the rocky cap on the central peak to the edge of the alluvial fans (as illustrated by the black lines in Figure 2f) was found to be 2.3 km and 1.5 km for the northern and western gullies/fans, respectively, and 780 m for the southern fan.

The northern fan emanates from the bottom of the gully measuring 110 m across and expands out to 1.1 km across at the base of the fan over a distance of 900 m. The deposits from the excavated gully at the base of the northern fan also intersect a dune field, and multiple smaller gully and fan features are in close proximity to the northern gully/fan, with some cross cutting others. This cross-cutting nature indicates a series of gully/fan formations transporting excavated material from the upper central uplift to the base in multiple, distinct episodes of activity. In comparison, the western fan emanates from the bottom of the western gully measuring 50 m across and expands out to 1 km across over a 600 m distance. Shown in Figure 2c, a smaller channel/fan is noticeable to the south on the central uplift that has a spectral signature comparable to the previous two fans (Figure 3). This smaller fan emanates directly from a rocky cap and fans out to 380 m over a 780 m distance.

An additional fan located on the western crater wall was identified (Figure 2b). Analysis of CRISM HRL000194F4 covering this fan suggests that the area lacks a clear hydrous mineral signature. CRISM images FRT00018405 and HRL0001B89D covering the crater ejecta did not show the presence of hydrous minerals.

3.2. Unnamed Elysium Impact Crater

Shown in Figure 4, the ~51 km diameter impact crater, known as 15-000018 in the *Robbins and Hynek* [2012] crater database, is a complex impact crater in Amazonian-Hesperian volcanic terrain [*Tanaka et al.*, 2014] located at 8.93°N, 141.28°E in the Elysium quadrangle of Mars. A recent study [*Sun and Milliken*, 2015] used crater counts to date this crater as 3.46 Ga, and thus, it is early Amazonian or late Hesperian aged [*Werner and Tanaka*, 2011]. The crater has slumped, terraced walls, a central uplift with an approximate diameter of 25 km and crater floor with dunes and sedimentary materials, interpreted to be later fill (Figure 4a). The ejecta is single layered, fluidized, and hummocky with broad lobes [*Robbins and Hynek*, 2012]. The crater floor has a minimum MOLA elevation of −4.05 km with an overall crater depth of 2.05 km with respect to the height of the crater rim. High-resolution imagery CTX P19_008305_1890 and HiRISE PSP_008305_1890 (shown in Figures 4b–4d) reveals that the floor of the crater to the south of the central uplift contains ~130 km^2 of eroded layered sedimentary deposits and dark dunes.

Five CRISM scenes cover the impact crater: FRT0000619D, FRT0000B0BE, FRT00017788, HRL000166A4, and HRS0000AB65. Summary parameters derived from FRT0000619D suggest the presence of Fe/Mg-rich phyllosilicates in the eroded relict sedimentary layers on the central uplift of the impact crater (Figures 4c and 4d). This is further corroborated through spectral analysis of the CRISM data, which reveals 1.92–1.93 μm H_2O absorptions along with 2.29–2.31 μm Fe and Mg-OH absorptions (Figure 5).

3.3. Stokes Impact Crater

The ~62 km diameter Stokes complex impact crater (07-000008 in the *Robbins and Hynek* [2012] crater database) is a complex impact crater located at 55.62 N, 171.23E within the Cebrenia quadrangle of Mars.

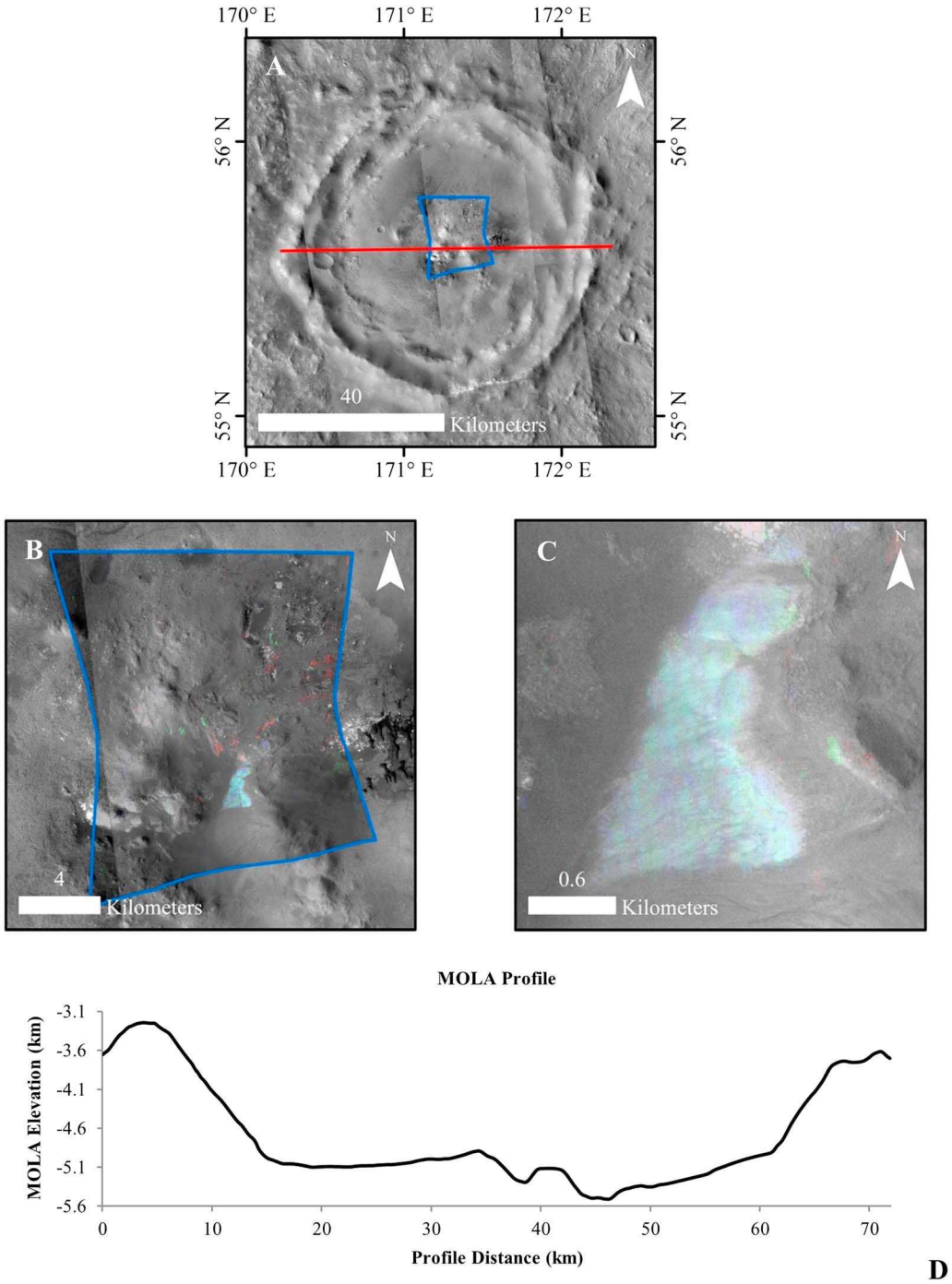

Figure 6. Complex impact crater Stokes located 55.62°N, 171.29°E of diameter 62 km. (a) CTX mosaic showing the impact crater with CRISM FRT0000ADA4 outline (blue) and location of the MOLA profile (red) overlain. (b) CTX mosaic with CRISM FRT0000ADA4 RGB parameter map [*Pelkey et al*., 2007] composite D2300 (red), BD2210 (green), and BD1900 (blue) overlain and color merged. (c) Image extracted from Figure 6b showing areas of mixed absorptions by RGB parameter maps (1.9 μm and 2.21 μm highlighted by cyan). (d) MOLA profile of impact crater shown in Figure 6a.

The terrain impacted is mapped as an Amazonian-Hesperian aged unit [*Tanaka et al*., 2014] and a recent study used crater counts to place an upper bound on this crater age 3.75 Ga [*Sun and Milliken*, 2015]. As seen in Figures 6a and 6b, the central uplift of Stokes crater is highly fractured, the crater floor has slump deposits derived from the crater walls, and the ejecta is radial, double layered, and hummocky with broad lobes, as previously stated by *Robbins and Hynek* [2012].

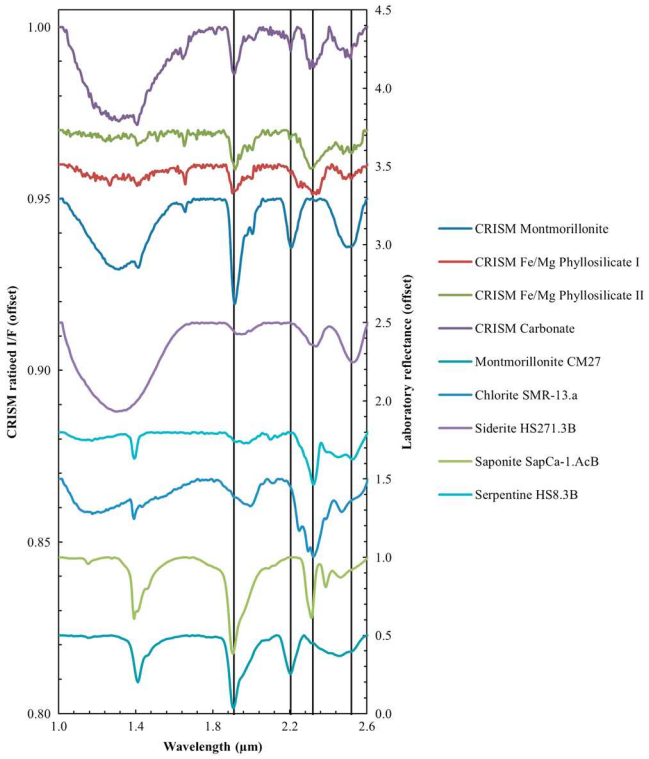

Figure 7. Comparisons of extracted spectra from FRT0000ADA4 covering Stokes impact crater shown in Figure 6 and spectra from the USGS Spectral Library [*Clark et al.*, 2007]. All extracted CRISM spectra have an absorption at ~1.91 μm. Additional absorptions are found for CRISM Montmorillonite at 2.2054 μm, CRISM Fe/Mg phyllosilicate I at 2.25 and 2.33 μm, CRISM Fe/Mg phyllosilicate II at 2.31 μm, and CRISM carbonate at 2.33 and 2.52 μm. All extracted spectra have an absorption at 2.5 μm, indicating an intermixed phase. USGS Spectra for Montmorillonite CM27, Chlorite SMR-13.a, Saponite SapCa-1.AcB, Serpentine HS8.3B, and Siderite HS271.3B.

A previous CRISM investigation of this crater (scene FRT0000ADA4) detected Fe-Mg phyllosilicate, chlorite, and the Al phyllosilicates montmorillonite ($(Na,Ca)_{0.33}(Al,Mg)_2(Si_4O_{10})(OH)_2 \cdot nH_2O$) and kaolinite ($Al_2Si_2O_5(OH)_4$), along with pyroxene and olivine in and around the fractured central uplift [*Carter et al.*, 2010]. Similar observations have been made in this study, although additional minerals have also been detected. Figure 7 compares four spectra extracted from CRISM FRT0000ADA4 with spectra from the USGS Spectral Library. All CRISM-extracted spectra have an absorption at ~1.91 μm. Montmorillonite has been identified with an Al-OH absorption extending 2.15–2.28 μm centered at 2.2054 μm, as previously identified by *Carter et al.* [2010], although the terrains we sampled also have strong ~2.5 μm absorption not typical of montmorillonite, indicating an intermixed hydrated phase, possibly a hydrated salt or zeolite. Fe/Mg-rich phyllosilicate, comparable to chlorite, has been identified by an absorption at 2.33 μm with a shoulder at 2.25 μm, as previously identified by *Carter et al.* [2010]. Another Fe/Mg-rich phyllosilicate is identified by a 2.31 μm absorption. Finally, a spectrum comparable to the carbonate siderite was identified by absorptions at 2.33 μm and 2.52 μm. CRISM coverage of the crater ejecta (FRT00008A1E, HRL000183FB, HRL000194A3, and HRS0001B728) proved inconclusive for the identification of hydrous minerals. Both the present study and that of *Carter et al.* [2010] suggest the presence of alteration minerals within the central uplift of the crater, but absence in the ejecta surrounding the crater.

4. Discussion

A previous investigation of hydrated deposits detected in nine impact craters located in the northern lowlands concluded that the bulk of large diameter impact craters in the northern plains expose the prealtered Noachian basement [*Carter et al.*, 2010, 2013]. The distinction between excavation and impact-induced alteration is dependent on the location of the hydrated minerals within the impact crater. Occurrences of impact-induced, hydrated mineralization are expected in and around the central uplift and lower crater walls, whereas excavated hydrated minerals would lead to deposits of hydrated minerals in the central uplift walls and also in the crater ejecta [*Abramov and Kring*, 2005; *Ehlmann et al.*, 2011b]. In the case of this study, each impact crater was carefully considered for the arguments of preimpact- versus postimpact-induced hydrothermal alteration.

4.1. Unnamed Ismenius Lacus Impact Crater

For the unnamed impact crater in the Ismenius Lacus quadrangle shown in section 3.1, it is possible that the observed Fe/Mg phyllosilicates formed within the central uplift and were subsequently excavated, transported, and deposited by the processes that led to the formation of the gullies and alluvial fans—by a process

of physical weathering. The source of the gullies can also clearly be tracked to rocky alcoves on the central peak that have spectral signatures consistent with Fe/Mg phyllosilicates (Figure 3). Megabreccia blocks on the central uplift also have spectral signatures suggestive of Fe/Mg phyllosilicates. As shown in the results these Fe/Mg phyllosilicate minerals are likely to be Fe serpentine or chlorite, possibly with prehnite.

The relatively juvenile nature of the alluvial fan with no surface impact craters means that chemical weathering on the surface is unlikely to be the origin of the secondary minerals. The two alluvial fans differ from previous findings in that they emanate from gullies that do not appear on equator-facing slopes as suggested by previous studies for gullies at this latitude [*Heldmann et al*., 2007]. In this study, gullies have been observed on pole-, eastern, and western facing slopes with slopes ranging from 3.3° to 14.7°. In comparison, a previous study showed that gully formation in the 30°–45°S latitude region typically requires steep slopes as 87% of detected gullies have formed on slopes $>$21° [*Dickson et al*., 2007]. As detailed above, the network of channels comprising the northern and western facing gullies can be tracked back to a rocky cap on the central peak (Figure 2d). This suggests a prolonged, perhaps episodic, period of gully and fan formation, implying that such fans are not the result of one event alone, which is consistent with other studies of gully systems in impact craters [*Schon et al*., 2009]. At the northern base of the central uplift, the fan deposits are obscured by an overlying dune field. A fan angle of repose of $>$26° [*Heldmann and Mellon*, 2004] and gully and alluvial morphology indicate that formation by a dry mass-wasting process is unlikely. The intact state of the gully and fan differ from others found in the northern hemisphere where the majority tend to be eroded [*Heldmann et al*., 2007], indicating that the gullies found in Figure 3 are young in comparison.

The location of the phyllosilicate minerals—within alluvial fans, gullies, and megabreccia blocks on the central uplift—suggests a postimpact alteration process, although preimpact formation and subsequent excavation cannot be ruled out with 18 m scale orbital reflectance data alone. The lack of hydrous minerals in the crater walls and, more importantly, ejecta further suggests the possibility of an impact-induced hydrothermal system. The Fe/Mg phyllosilicates—likely Fe serpentine or chlorite—detected in the alluvial fans and gullies may have formed in the subsurface of the central uplift where the circulation of hydrothermal fluids might have been present postimpact. Then, these altered deposits were since excavated, eroded, and transported by the gully system to the alluvial fans at the base of the central uplift. We favor this model of recent redistribution of hydrated minerals, but alternatively, the central peak may have discharged waters through the central peak to form the channels and alluvial fans. If prehnite is present, then it would indicate alteration at elevated temperatures of 200–350°C [*Robinson and Bevins*, 1999].

4.2. Unnamed Elysium Impact Crater

The unnamed Elysium impact crater in section 3.2 exhibits hydrated minerals in heavily eroded sediments around the southwest region of the central uplift. No hydrated minerals are found around the crater rim or in the ejecta. The interior sediments appear to postdate the formation of the crater with no obvious link to the crater's formation or potential impact hydrothermal history. They may be analogous to interior layered deposits frequently found in large craters, notably within Arabia Terra. The clay minerals may have formed in place through diagenesis, similar to that in Gale crater [*Bridges et al*., 2015] or have formed outside the crater and been deposited. The hydrated minerals found here are unlikely to be the result of impact-induced hydrothermal alteration.

4.3. Stokes Impact Crater

In section 3.3, the spectra of Stokes impact crater show no clear evidence of absorptions due to hydrous minerals in the crater ejecta. Nevertheless, previous work concluded that all hydrated minerals formed preimpact due to the proximity of a suite of alteration minerals (serpentine, chlorite, nontronite, and kaolinite) to unaltered olivine and pyroxene within the central structure of the crater [*Carter et al*., 2010]. The analysis of Stokes crater was part of a study that showed nine craters in the northern plains host hydrated silicates, and the conclusion of excavation applied to the group of craters as a whole because only the largest of the craters, which had the capacity to excavate beneath post Noachian units, had signatures of hydrated minerals [*Carter et al*., 2010]. Studies have shown that Al phyllosilicates might form as a result of impact-induced hydrothermal alteration [*Schwenzer and Kring*, 2009]. Al phyllosilicates have been found by MER Opportunity at Endeavor crater, along with Fe smectites [*Arvidson et al*., 2014]. Previous studies of Majuro and Toro impact craters have demonstrated how the link between hydrated minerals and the central uplift

can help in identifying impact-induced hydrothermal systems [*Marzo et al*., 2010; *Mangold et al*., 2012]. The Al phyllosilicate, possibly montmorillonite, is detected on a large outcrop within the fractured central uplift of Stokes crater (Figure 6c). Either formation postimpact or excavation are permitted; orbital reflectance data at 18 m per pixel resolution cannot distinguish.

4.4. Comparisons With Previous Studies

Fe/Mg phyllosilicates in the central peak but not the upper walls and ejecta are consistent with impact-induced hydrothermal models for complex impact craters in which serpentine, chlorite, and nontronite ($Na_{0.3}Fe_2^{3+}(Si,Al)_4O_{10}(OH)_2 \cdot nH_2O$) are predicted to occur on central uplifts [*Schwenzer and Kring*, 2009, 2013]. Clearly, impact excavation from depth could also produce hydrated minerals in the central peak. In the absence of a mechanism for masking the spectral signature of excavated materials in the walls and ejecta but not in the central uplift, the most logical explanation is postimpact formation of the hydrated minerals. However, one mechanism for masking signatures could be higher topographic relief in the central peak resulting in more active erosion leaving the minerals exposed and free of dust cover compared to the crater walls and ejecta.

Previous studies reported that 19 impact craters out of a sample of 100 show hydrated minerals in the northern plains and concluded that these hydrated minerals were excavated from preexisting underlying layers dating from the Noachian, based on depth-to-diameter relations [*Carter et al*., 2010, 2013]. However, on the basis of our results, it is evident that each crater must be individually analyzed in detail in order to determine the exact origin of hydrated minerals. We conclude that 1–2 of the 158 post Noachian craters may host hydrated minerals formed by impact-induced hydrothermal activity. Another recent study of clays on crater central peaks found that 10 Amazonian-aged impact craters showed evidence for hydrated minerals, and four craters had clays solely in impact melt units [*Sun and Milliken*, 2015]. The study by *Sun and Milliken* [2015] differs from this one by studying a global population of 633 impact craters on Mars and then using crater counts to determine the age of each crater, rather than using superposition relationships with terrains mapped and craters counted for the latest USGS geologic map of Mars, as in this study.

Our results suggest that impact-induced hydrothermal alteration may be associated with the central uplifts of the unnamed Ismenius Lacus impact crater and Stokes impact crater, implying post Noachian impact hydrothermalism. Previous studies have found evidence for impact-induced hydrothermal alteration in Hesperian-aged Majuro [*Mangold et al*., 2012] crater and suggested for the Noachian-aged Holden crater [*Grant et al*., 2008; *Tornabene et al*., 2009; *Osinski et al*., 2013] and the Hesperian-aged Toro crater [*Marzo et al*., 2010]. Moreover, meteorite data from the Amazonian-aged SNCs suggest that minor amounts of postimpact alteration occurred [*Changela and Bridges*, 2010; *Bridges and Schwenzer*, 2012; *Hicks et al*., 2014].

4.5. Low Abundance of Impact-Induced Hydrothermal Systems

Multiple causes are possible for the apparent rarity of impact-induced hydrothermal systems within complex post Noachian, and in particular Amazonian, impact craters (diameter $>$7 km). First, such systems may in fact have rarely occurred, limited by the availability of liquid water. Second, the paucity of identified systems could be the result of the lack of surface exposure of alteration minerals, since impact-induced hydrothermal systems are predominantly subsurface processes, and moreover, underlying lithology is frequently obscured from remote sensing by dust cover. In some regions on Mars (e.g., Tharsis) dust coverage is extensive, particularly in younger Amazonian-aged terrains, therefore limiting the use of reflectance spectroscopy. Extensive crater infilling by sediments after impact-induced hydrothermal systems ceased would also obscure impact-associated hydrothermalism. Third, the abundance of alteration minerals could be relatively small in typical Amazonian hydrothermal systems, as exemplified by the abundance of alteration phases in the nakhlite meteorites [e.g., *Changela and Bridges*, 2010]. The presence of hydrated phases at a few weight percent abundance or less is not readily discernible in infrared remote sensing data sets. These hydrothermal systems causing little or spatially confined alteration would be impossible to detect with current remote sensing capabilities. Finally, the proportion of craters with high-resolution CRISM coverage is relatively small, which means that the proportion of Amazonian craters that have experienced hydrothermal activity as a result of an impact could be underestimated.

The dominant heat source for a complex impact crater depends on crater size. For impact craters $\geq$7 km and $<$130 km this is the central uplift, whereas in larger diameter impact craters ($>\sim$130 km) the dominant heat

source is the impact melt rather than the central uplift. Nevertheless, the central uplift is still important as it raises the underlying geothermal gradient [*Daubar and Kring*, 2001]. In contrast, for smaller, simple craters (diameter $<$7 km) the dominant heat source is shock-emplaced heat that may result in short-lived alteration of the Martian crust [*Schwenzer and Kring*, 2013]. The smaller crater survey was included in this study in an attempt to identify alteration minerals in such impact craters; however, no hydrated minerals were identified. This lack of hydrated signatures could be due to a number of reasons: (a) no alteration took place; (b) alteration was restricted to the unexposed subsurface; (c) dust coverage may be masking spectral signatures; (d) the mineral outcrops are not sizable enough for CRISM to resolve; or (e) the alteration minerals are of low abundance.

4.6. Technical Limitations of This Study

This study highlights the current limitations in identifying impact-induced hydrothermal systems on Mars and analogues (or source regions) for the Martian meteorites. Current remote sensing technologies to determine surface composition (i.e., OMEGA and CRISM) use reflectance spectroscopy and are unable to probe more than a millimeter beneath the surface, relying on erosion to expose bedrock and materials of interest for sensing. As previously stated, another limitation to consider is the ~20 m/pixel resolution of CRISM as some mineral outcrops may not be sizable enough to resolve at that scale. Nevertheless, CRISM has been able to provide a detailed surface mineralogy of Mars [e.g., *Murchie et al*., 2009a; *Carter et al*., 2013]. However, analysis of the CRISM data set is hampered by spectral artifacts such as spurious pixels caused by detector temperature [*Murchie et al*., 2009b]. The standard approach of analyzing CRISM data using spectral ratios (as used in this study) works well to divide out most spectral artifacts, although some still do persist [*Murchie et al*., 2009b]. More complex statistics-based analysis using principal components analysis and minimum noise transformation was explored during this study but these techniques were found to be inapplicable to the data set due to the systematic column-to-column differences and the presence of random noise.

4.7. Relevance to the Nakhlites

Previous work linking the nakhlite alteration assemblages to impact-induced hydrothermal systems has suggested that the size and age of craters examined in this study are those where such a mineral assemblage could have been produced [*Changela and Bridges*, 2010; *Bridges and Schwenzer*, 2012]. Links between the laboratory-based studies on Earth of the nakhlites [*Changela and Bridges*, 2010; *Hicks et al*., 2014] and remote sensing studies of Mars have limitations as the nakhlites were excavated from the subsurface. Small amounts of alteration like those seen in the nakhlites, e.g., ~$\leq$1 wt % may very well be undetectable in orbital infrared data, based on laboratory study of nakhla bulk rock spectra [*Hamilton et al*., 1997; *Schade and Wasch*, 1999]. However, the secondary minerals identified here (i.e., Fe/Mg phyllosilicates) are similar to those of the nakhlites and may have a similar impact-associated origin.

5. Conclusions

1. This study conducted CRISM analysis of 144 craters of $\geq$7 km diameter in terrains mapped as Amazonian or Amazonian-Hesperian on Mars. This search was mainly performed in the northern lowlands with a further search around Hellas Basin; however, no CRISM coverage was available for the Hellas region. Hydrated minerals in these impact craters appear scarce, with only 3 out of 144 craters in this study showing spectral signs of such minerals.
2. Gullies, alluvial fans, and uplifted breccia in the central uplift of an unnamed 20 km diameter impact crater (located at 52.42°N, 39.86°E in the Ismenius Lacus quadrangle) show spectral evidence for a chlorite or Fe serpentine that may have formed through erosion and redeposition of impact-induced hydrothermal mineral assemblages during the Amazonian epoch.
3. Fe/Mg/Al phyllosilicates, chlorite, and carbonate in the 62 km diameter Stokes impact crater may be the result of impact-induced hydrothermal alteration.
4. Excavation of older, preimpact altered, Noachian terrains cannot be ruled out as a potential origin for the hydrated minerals found in this study.
5. A small crater survey concluded that 14 simple impact craters of diameters $\geq$3 km and $<$7 km in relatively dust-free Amazonian terrains in the Northern plains lack hydrated minerals in available CRISM data.
6. Our work suggests that hydrothermalism was rare in the Amazonian or not extensive enough to be detectable at CRISM spatial scale.

Acknowledgments
Turner was funded by a joint STFC-NERC (British Geological Survey) CASE studentship. Grebby publishes with the permission of the Executive Director, British Geological Survey (NERC). We would like to thank MRO and MOLA science teams for their work in acquiring and processing the data. CRISM data used in this paper are available from the NASA Planetary Data System Geoscience Node (http://pds-geosciences.wustl.edu/missions/mro/crism.htm), HiRISE images are available from the University of Arizona HiRISE website (https://hirise.lpl.arizona.edu/), CTX images are available from the Image Explorer on the Arizona State University website (http://viewer.mars.asu.edu/viewer/ctx#T=0), and MOLA data are available from the United States Geological Survey Planetary GIS Web Server (http://webgis.wr.usgs.gov/pigwad/down/mars_dl.htm). We thank Cong Pan and an anonymous reviewer for their comments.

References

Abramov, O., and D. A. Kring (2005), Impact-induced hydrothermal activity on early Mars, *J. Geophys. Res.*, *110*, E12S09, doi:10.1029/2005JE002453.

Adams, J. B. (1975), Interpretation of visible and near-infrared diffuse reflectance spectra of pyroxenes and other rock-forming minerals, in *Infrared Raman Spectroscopy of Lunar and Terrestrial Minerals*, pp. 91–116, Academic Press, London.

Arvidson, R. E., et al. (2014), Ancient aqueous environments at Endeavour crater, Mars, *Science*, *343*, doi:10.1126/science.1248097.

Barnhart, C. J., F. Nimmo, and B. J. Travis (2010), Martian post-impact hydrothermal systems incorporating freezing, *Icarus*, *208*, 101–117.

Bibring, J.-P., Y. Langevin, J. F. Mustard, F. Poulet, R. Arvidson, A. Gendrin, B. Gondet, N. Mangold, P. Pinet, and F. Forget (2006), Global mineralogical and aqueous Mars history derived from OMEGA/Mars Express data, *Science*, *312*, 400–404, doi:10.1126/science.1122659.

Bish, D., et al. (2014), The first X-ray diffraction measurements on Mars, *IUCrJ*, *1*, 514–522, doi:10.1107/S2052252514021150.

Bishop, J. L., E. Murad, and M. D. Dyar (2002b), The influence of octahedral and tetrahedral cation substitution on the structure of smectites and serpentines as observed through infrared spectroscopy, *Clay Miner.*, *37*, 617–628, doi:10.1180/0009855023740064.

Bishop, J. L., M. D. Lane, M. D. Dyar, and A. J. Brown (2008), Reflectance and emission spectroscopy of four groups of phyllosilicates: Smectites, kaolinite-serpentines, chlorites, and micas, *Clay Miner.*, *43*, 35–54, doi:10.1180/claymin.2008.043.1.03.

Bishop, J., J. Madejova, P. Komadel, and H. Froschl (2002a), The influence of structural Fe, Al, and Mg on the infrared OH bands in spectra of dioctahedral smectites, *Clay Miner.*, *37*, 607–616, doi:10.1180/0009855023740063.

Bridges, J. C., and M. M. Grady (2000), Evaporite mineral assemblages in the nakhlite (Martian) meteorites, *Earth Planet. Sci. Lett.*, *176*(3), 267–279.

Bridges, J. C., and S. P. Schwenzer (2012), The nakhlite hydrothermal brine on Mars, *Earth Planet. Sci. Lett.*, *359–360*, 117–123.

Bridges, J. C., S. P. Schwenzer, R. Leveille, F. Westall, R. C. Wiens, N. Mangold, T. Bristow, P. Edwards, and G. Berger (2015), Diagenesis and clay mineral formation at Gale Crater, Mars, *J. Geophys. Res. Planets*, *120*, 1–19, doi:10.1002/2014JE004757.

Bultel, B., C. Quantin-Nataf, M. Andréani, H. Clénet, and L. Lozac'h (2015), Deep alteration between Hellas and Isidis Basins, *Icarus*, *260*, 141–160, doi:10.1016/j.icarus.2015.06.037.

Burns, R. G. (1970), *Mineralogical Applications of Crystal Field Theory*, Cambridge Univ. Press, London.

Carter, J., and F. Poulet (2012), Orbital identification of clays and carbonates in Gusev crater, *Icarus*, *219*, 250–253, doi:10.1016/j.icarus.2012.02.024.

Carter, J., F. Poulet, J.-P. Bibring, and S. Murchie (2010), Detection of hydrated silicates in crustal outcrops in the northern plains of Mars, *Science*, *328*, 1682–1686, doi:10.1126/science.1189013.

Carter, J., F. Poulet, J.-P. Bibring, N. Mangold, and S. Murchie (2013), Hydrous minerals on Mars as seen by the CRISM and OMEGA imaging spectrometers: Updated global view, *J. Geophys. Res. Planets*, *118*, 831–858, doi:10.1029/2012JE004145.

Changela, H. G., and J. C. Bridges (2010), Alteration assemblages in the nakhlites: Variation with depth on Mars, *Meteorit. Planet. Sci.*, *45*, 1847–1867.

Clark, R. N., G. A. Swayze, R. Wise, K. E. Livo, T. M. Hoefen, R. F. Kokaly, and S. J. Sutley (2007), USGS digital spectral library splib06a, U.S. Geol. Surv. Data, 231.

Cloutis, E. A., et al. (2006), Detection and discrimination of sulfate minerals using reflectance spectroscopy, *Icarus*, *184*, 121–157, doi:10.1016/j.icarus.2006.04.003.

Cockell, C. S., M. Balme, J. C. Bridges, A. Davila, and S. P. Schwenzer (2012), Uninhabited habitats on Mars, *Icarus*, *217*, 184–193, doi:10.1016/j.icarus.2011.10.025.

Daubar, I. J., and D. A. Kring (2001), Impact-induced hydrothermal systems: Heat sources and lifetimes, In Lunar and Planetary Institute Science Conference Abstracts, volume 32 of Lunar and Planetary Institute Science Conference Abstracts, page 1727.

Dickson, J. L., J. W. Head, and M. Kreslavsky (2007), Martian gullies in the southern mid-latitudes of Mars: Evidence for climate-controlled formation of young fluvial features based upon local and global topography, *Icarus*, *188*(2), 315–323.

Ehlmann, B. L., and C. S. Edwards (2014), Mineralogy of the Martian surface, *Annu. Rev. Earth Planet. Sci.*, *42*, 291–315, doi:10.1146/annurev-earth-060313-055024.

Ehlmann, B. L., et al. (2008), Orbital identification of carbonate-bearing rocks on Mars, *Science*, *322*, 1828–1832, doi:10.1126/science.1164759.

Ehlmann, B. L., et al. (2009), Identification of hydrated silicate minerals on Mars using MRO-CRISM: Geologic context near Nili Fossae and implications for aqueous alteration, *J. Geophys. Res.*, *114*, E00D08, doi:10.1029/2009JE003339.

Ehlmann, B. L., J. F. Mustard, R. N. Clark, G. A. Swayze, and S. L. Murchie (2011a), Evidence for low-grade metamorphism, hydrothermal alteration, and diagenesis on Mars from phyllosilicate mineral assemblages, *Clays Clay Miner.*, *590*(4), 359–377, doi:10.1346/CCMN.2011.0590402.

Ehlmann, B. L., J. F. Mustard, S. L. Murchie, J.-P. Bibring, A. Meunier, A. A. Fraeman, and Y. Langevin (2011b), Subsurface water and clay mineral formation during the early history of Mars, *Nature*, *479*, 53–60, doi:10.1038/nature10582.

Filiberto, J., and S. P. Schwenzer (2013), Alteration mineralogy of Home Plate and Columbia Hills-Formation conditions in context to impact, volcanism, and fluvial activity, *Meteorit. Planet. Sci.*, *48*, 1937–1957, doi:10.1111/maps.12207.

Gaffey, S. J. (1987), Spectral reflectance of carbonate minerals in the visible and near infrared (0.35–2.55 um): Anhydrous carbonate minerals, *J. Geophys. Res.*, *92*, 1429–1440, doi:10.1029/JB092iB02p01429.

Gooding, J. L., S. J. Wentworth, and M. E. Zolensky (1991), Aqueous alteration of the Nakhla meteorite, *Meteoritics*, *26*, 135–143, doi:10.1111/j.1945-5100.1991.tb01029.x.

Grant, J. A., R. P. Irwin, J. P. Grotzinger, R. E. Milliken, L. L. Tornabene, A. S. McEwen, C. M. Weitz, S. W. Squyres, T. D. Glotch, and B. J. Thomson (2008), HiRISE imaging of impact megabreccia and sub-meter aqueous strata in Holden Crater, Mars, *Geology*, *36*, 195–198, doi:10.1130/G24340A.1.

Gross, C., L. Wendt, J.-P. Combe, P. Jodlowski, G. A. Marzo, T. L. Roush, T. McCord, P. Halbach, and G. Neukum (2012), Investigating the phyllosilicate bearing Micoud crater in the northern plains of Mars In Lunar and Planetary Institute Science Conference Abstracts, volume 43 of Lunar and Planetary Institute Science Conference Abstracts, page 1795.

Grotzinger, J. P., et al. (2014), A habitable fluvio-lacustrine environment at Yellowknife Bay, Gale Crater, Mars, *Science*, *343*, doi:10.1126/science.1242777.

Hamilton, V. E., P. R. Christensen, and H. Y. McSween Jr. (1997), Determination of Martian meteorite lithologies and mineralogies using vibrational spectroscopy, *J. Geophys. Res.*, *102*(E11), 25,593–25,603, doi:10.1029/97JE01874.

Head, J. N., H. J. Melosh, and B. A. Ivanov (2002), Martian meteorite launch: High-speed ejecta from small craters, *Science*, *298*(5599), 1752–1756.

Heldmann, J. L., and M. T. Mellon (2004), Observations of Martian gullies and constraints on potential formation mechanisms, *Icarus*, *168*(2), 285–304.

Heldmann, J. L., E. Carlsson, H. Johansson, M. T. Mellon, and O. B. Toon (2007), Observations of Martian gullies and constraints on potential formation mechanisms: II The northern hemisphere, *Icarus*, *188*(2), 324–344.

Hicks, L. J., J. C. Bridges, and S. J. Gurman (2014), Ferric saponite and serpentine in the nakhlite Martian meteorites, *Geochim. Cosmochim. Acta*, *136*, 194–210, doi:10.1016/j.gca.2014.04.010.
Langevin, Y., J.-P. Bibring, F. Montmessin, F. Forget, M. Vincendon, S. Douté, F. Poulet, and B. Gondet (2007), Observations of the south seasonal cap of Mars during recession in 2004–2006 by the OMEGA visible/near-infrared imaging spectrometer on board Mars Express, *J. Geophys. Res.*, *112*, E08S12, doi:10.1029/2006JE002841.
Malin, M. C., et al. (2007), Context camera investigation on board the Mars Reconnaissance Orbiter, *J. Geophys. Res.*, *112*, E05S04, doi:10.1029/2006JE002808.
Mangold, N., J. Carter, F. Poulet, E. Dehouck, V. Ansan, and D. Loizeau (2012), Late Hesperian aqueous alteration at Majuro crater, Mars, *Planet. Space Sci.*, *72*, 18–30, doi:10.1016/j.pss.2012.03.014.
Marzo, G. A., A. F. Davila, L. L. Tornabene, J. M. Dohm, A. G. Fairén, C. Gross, T. Kneissl, J. L. Bishop, T. L. Roush, and C. P. McKay (2010), Evidence for Hesperian impact-induced hydrothermalism on Mars, *Icarus*, *208*, 667–683, doi:10.1016/j.icarus.2010.03.013.
McEwen, A. S., et al. (2007), Mars reconnaissance orbiter's high Resolution Imaging Science Experiment (HiRISE), *J. Geophys. Res.*, *112*, E05S02, doi:10.1029/2005JE002605.
McGuire, P. C., et al. (2009), An improvement to the volcano-scan algorithm for atmospheric correction of CRISM and OMEGA spectral data, *Planet. Space Sci.*, *57*, 809–815, doi:10.1016/j.pss.2009.03.007.
McLennan, S. M., et al. (2014), Elemental geochemistry of sedimentary rocks in Yellowknife Bay, Gale Crater, Mars, *Science*, *343*, doi:10.1126/science.1244734.
Melosh, H. J. (1989), *Impact Cratering: A Geologic Process*, Oxford Univ. Press, New York.
Milliken, R. E., J. P. Grotzinger, and B. J. Thomson (2010), Paleoclimate of Mars as captured by the stratigraphic record in Gale Crater, *Geophys. Res. Lett.*, *37*, L04201, doi:10.1029/2009GL041870.
Ming, D. W., et al. (2006), Geochemical and mineralogical indicators for aqueous processes in the Columbia Hills of Gusev crater, Mars, *J. Geophys. Res.*, *111*, E02S12, doi:10.1029/2005JE002560.
Morris, R. V., et al. (2010), Identification of carbonate-rich outcrops on Mars by the Spirit Rover, *Science*, *329*, 421–424, doi:10.1126/science.1189667.
Murchie, S., et al. (2007), Compact Reconnaissance Imaging Spectrometer for Mars (CRISM) on Mars Reconnaissance Orbiter (MRO), *J. Geophys. Res.*, *112*, E05S03, doi:10.1029/2006JE002682.
Murchie, S. L., et al. (2009a), A synthesis of Martian aqueous mineralogy after 1 Mars year of observations from the Mars reconnaissance Orbiter, *J. Geophys. Res.*, *114*, E00D06, doi:10.1029/2009JE003342.
Murchie, S. L., et al. (2009b), Compact Reconnaissance Imaging Spectrometer for Mars investigation and data set from the Mars reconnaissance orbiter's primary science phase, *J. Geophys. Res.*, *114*, E00D07, doi:10.1029/2009JE003344.
Mustard, J. F., F. Poulet, A. Gendrin, J.-P. Bibring, Y. Langevin, B. Gondet, N. Mangold, G. Bellucci, and F. Altieri (2005), Olivine and pyroxene diversity in the crust of Mars, *Science*, *307*, 1594–1597, doi:10.1126/science.1109098.
Mustard, J. F., et al. (2008), Hydrated silicate minerals on Mars observed by the CRISM instrument on MRO, *Nature*, *454*, 305–309, doi:10.1038/nature07097.
Nyquist, L. E., D. D. Bogard, C.-Y. Shih, A. Greshake, D. Stoffler, and O. Eugster (2001), Ages and geologic histories of Martian meteorites, *Space Sci. Rev.*, *96*, 105–164.
Osinski, G. R., et al. (2013), Impact-generated hydrothermal systems on Earth and Mars, *Icarus*, *224*, 347–363, doi:10.1016/j.icarus.2012.08.030.
Pelkey, S. M., et al. (2007), CRISM multispectral summary products: Parameterizing mineral diversity on Mars from reflectance, *J. Geophys. Res.*, *112*, E08S14, doi:10.1029/2006JE002831.
Poulet, F., J.-P. Bibring, J. F. Mustard, A. Gendrin, N. Mangold, Y. Langevin, R. E. Arvidson, B. Gondet, and C. Gomez (2005), Phyllosilicates on Mars and implications for early Martian climate, *Nature*, *438*, 623–627, doi:10.1038/nature04274.
Poulet, F., C. Gomez, J.-P. Bibring, Y. Langevin, B. Gondet, P. Pinet, G. Belluci, and J. Mustard (2007), Martian surface mineralogy from Observatoire pour la Mineralogie, l'Eau, les Glaces et l'Activite on board the Mars Express spacecraft (OMEGA/MEx): Global mineral maps, *J. Geophys. Res.*, *112*, E08S02, doi:10.1029/2006JE002840.
Rathbun, J. A., and S. W. Squyres (2002), Hydrothermal systems associated with Martian impact craters, *Icarus*, *157*, 362–372.
Robbins, S. J., and B. M. Hynek (2012), A new global database of Mars impact craters ≥1 km: 1. Database creation, properties, and parameters, *J. Geophys. Res.*, *117*, E05004, doi:10.1029/2011JE003966.
Robinson, D., and R. E. Bevins (1999), Patterns of regional low-grade metamorphism in metabasites, in *Low-Grade Metamorphism*, edited by M. Frey and D. Robinson, pp. 143–168, Blackwell Sci, Oxford, U. K.
Ruff, S. W., and P. R. Christensen (2002), Bright and dark regions on Mars: Particle size and mineralogical characteristics based on Thermal Emission Spectrometer data, *J. Geophys. Res.*, *107*(E12), 5127, doi:10.1029/2001JE001580.
Schade, U., and R. Wasch (1999), Near-infared reflectance spectra from bulk samples of the two Martian meteorites Zagami and Nakhla, *Meteorit. Planet. Sci.*, *34*, 417–424.
Schon, S. C., J. W. Head, and C. I. Fassett (2009), Unique chrono-stratigraphic marker in depositional fan stratigraphy on Mars: Evidence for ca. 1.25 Ma gully activity and surficial meltwater origin, *Geology*, *37*, 207–210, doi:10.1130/G25398A.1.
Schwenzer, S. P., and D. A. Kring (2009), Impact-generated hydrothermal systems capable of forming phyllosilicates on Noachian Mars, *Geology*, *370*(12), 1091–1094, doi:10.1130/G30340A.1.
Schwenzer, S. P., and D. A. Kring (2013), Alteration minerals in impact-generated hydrothermal systems–Exploring host rock variability, *Icarus*, *226*(1), 487–496, doi:10.1016/j.icarus.2913.06.003.
Shih, C.-Y., L. E. Nyquist, Y. Reese, and H. Wiesmann (1998), The chronology of the Nakhlite, Lafayette: Rb-Sr and Sm-Nd Isotopic ages In Lunar and Planetary Institute Science Conference Abstracts, volume 29 of Lunar and Planetary Institute Science Conference Abstracts, page 1145.
Smith, D. E., et al. (2001), Mars orbiter laser altimeter: Experiment summary after the first year of global mapping on Mars, *J. Geophys. Res.*, *106*(E10), 23,689–23,722, doi:10.1029/2000JE001364.
Squyres, S. W., et al. (2004), In situ evidence for an ancient aqueous environment at Meridiani Planum, Mars, *Science*, *306*, 1709–1713, doi:10.1126/science.1104559.
Squyres, S. W., et al. (2008), Detection of silica-rich deposits on Mars, *Science*, *320*, 1063–1067, doi:10.1126/science.1155429.
Sun, V. Z., and R. E. Milliken (2014), The geology and mineralogy of Ritchey crater, Mars: Evidence for post Noachian clay formation, *J. Geophys. Res. Planets*, *119*, 810–836, doi:10.1002/2013JE004602.
Sun, V. Z., and R. E. Milliken (2015), Ancient and recent clay formation on Mars as revealed from a global survey of hydrated minerals in crater central peaks, *J. Geophys. Res. Planets*, *120*, 2293–2332, doi:10.1002/2015JE004918.

Swindle, T. D., A. H. Treiman, D. J. Lindstrom, M. K. Burkland, B. A. Cohen, J. A. Grier, B. Li, and E. K. Olson (2000), Noble gases in iddingsite from the Lafayette meteorite: Evidence for liquid water on Mars in the last few hundred million years, *Meteorit. Planet. Sci.*, *35*(1), 107–115, doi:10.1111/j.1945-5100.2000.tb01978.x.

Tanaka, K. L., S. J. Robbins, C. M. Fortezzo, J. A. Skinner, and T. M. Hare (2014), The digital global geologic map of Mars: Chronostratigraphic ages, topographic and crater morphologic characteristics, and updated resurfacing history, *Planet. Space Sci.*, *95*, 11–24, doi:10.1016/j.pss.2013.03.006.

Thomson, B. J., N. T. Bridges, R. Milliken, A. Baldridge, S. J. Hook, J. K. Crowley, G. M. Marion, C. R. de Souza Filho, A. J. Brown, and C. M. Weitz (2011), Constraints on the origin and evolution of the layered mound in Gale Crater, Mars using Mars Reconnaissance Orbiter data, *Icarus*, *214*, 413–432, doi:10.1016/j.icarus.2011.05.002.

Tornabene, L. L., G. R. Osinski, and A. S. McEwen (2009), Parautochthonous megabreccias and possible evidence of impact-induced hydrothermal alteration in Holden Crater, Mars, In Lunar and Planetary Institute Science Conference Abstracts, volume 40 of Lunar and Planetary Institute Science Conference Abstracts, page 1766.

Vaniman, D. T., et al. (2014), Mineralogy of a mudstone at Yellowknife Bay, Gale Crater, Mars, *Science*, *343*(6169), doi:10.1126/science.1243480.

Werner, S. C., and K. L. Tanaka (2011), Redefinition of the crater-density and absolute-age boundaries for the chronostratigraphic system of Mars, *Icarus*, *215*, 603–607.